JOURNAL OF MATERIALS SCIENCE **33** (1998) 5895–5899

Effect of the thickness of plasma-sprayed coating on bond strength and thermal fatigue characteristics

H. M. CHOI, B. S. KANG, W. K. CHOI, D. G. CHOI, S. K. CHOI
Department of Materials Science and Engineering, Korea Advanced Institute of Science and Technology, 373-1, Kusung-dong Yusung-gu Daejon 305-701, Korea
E-mail: s_choihm@kaist.ac.kr

J. C. KIM, Y. K. PARK
Power Generation Research Laboratory, Electric Power Research Institute, 103-16, Minji-dong Yusung-gu Daejon 305-380, Korea

G. M. KIM
Department of Materials Engineering, Chungnam National University, 220, Kung-dong Daejon 305-764, Korea

NiCrAlY bond coat and ZrO_2–8 wt % Y_2O_3 top coat with various thicknesses were deposited on Hastelloy X by plasma spraying. Residual stress was calculated by the finite element method (FEM) to explain the variations in the bond strength and thermal fatigue characteristics with the thickness of the bond coat and top coat. The bond strength of thermal barrier coatings (TBCs) increased with decreasing maximum residual stress in the *y*-direction of the top coat. The thermal fatigue characteristics increased with decrease of the maximum principal residual stress of the top coat and the thickness of oxidation layer of the bond coat.

1. Introduction

Plasma spraying has been used to deposit thermal barrier coatings (TBCs) for gas turbine applications. TBC should achieve both a high level of insulation and a low level of interfacial expansion mismatch stress. These criteria have been met by yttria-stabilized zirconia with a relatively low thermal conductivity and high thermal expansion coefficient [1].

Material selection, porosity control and other important parameters are needed to obtain high-level insulation, but the easiest way is to increase the coating thickness. However, TBC should achieve not only high-level insulation [2–4], but also high bond strength and good thermal fatigue resistance [5–8] which are also affected by the coating thickness.

In this study, NiCrAlY bond coat and 8 wt % yttria-stabilized zirconia top coat with various thicknesses were deposited by plasma spraying to investigate the effect of the thickness of the bond coat and top coat on the bond strength and the thermal fatigue characteristics. Residual stress of the top coat was calculated by the finite element method (FEM) and the results used to explain the relationship between the thicknesses of the bond coat and top coat and bond strength and thermal fatigue characteristics. The result of FEM was confirmed by measuring the residual stress in the top coat by X-ray diffraction (XRD).

2. Experimental procedure

NiCrAlY (AMDRY 962) bond coat and ZrO_2–8 wt % Y_2O_3 (METCO 204NS) top coat were deposited on Hastelloy X by plasma spraying (METCO). Tables I and II show the deposition conditions of bond coat and top coat, respectively. Table III shows the thickness of the deposited bond coat and top coat. The scan number was controlled to vary the thickness of the bond coat and top coat. B1T4 in Table III indicates one scan of the bond coat and four scans of the top coat.

Scanning electron microscopy (SEM) and energy dispersive spectroscopy (EDS)/wavelength dispersive spectroscopy (WDS) were used to measure the thickness of the bond coat and top coat and to analyse the composition of the deposited bond coat and top coat, respectively. Thermal conductivity of the top coat was also measured by the laser flash method [9,10] to evaluate the basic property of the top coat.

The crystal structure of the top coat was analysed by X-ray diffractometer (Rigaku, D/MAX-RC) with monochromatic CuK_α radiation generated at 40 kV and 100 mA.

A tensile test (Instron 4206) was carried out to measure bond strength. The samples for tensile testing were prepared by attaching the coated samples (25 mm × 25 mm × 3 mm) to a jig with epoxy [2–4].

0022–2461

TABLE I Deposition conditions for the bond coat

Voltage (V)	75
Current (A)	500
Primary gas flow rate Ar (l min^{-1})	38
Secondary gas flow rate H_2 (l min^{-1})	9
Carrier gas Ar (l min^{-1})	17
Spraying distance (mm)	140
Substrate cooling	No cooling

TABLE II Deposition conditions for the top coat

Voltage (V)	67
Current (A)	600
Primary gas flow rate Ar (l min^{-1})	38
Secondary gas flow rate H_2 (l min^{-1})	5
Carrier gas Ar (l min^{-1})	17
Spraying distance (mm)	64
Substrate cooling	No cooling

TABLE III Thickness of the deposited thermal barrier coatings

	Sample name					
	B1T4	B2T4	B3T4	B2T2	B2T4	B2T6
Scan number (bond coat)	1(B1)	2(B2)	3(B3)	2(B2)	2(B2)	2(B2)
Thickness (μm)	61	120	138	120	120	120
Scan number (top coat)	4(T4)	4(T4)	4(T4)	2(T2)	4(T4)	6(T6)
Thickness (μm)	346	269	384	120	269	423

The samples were thermally cycled to estimate the thermal fatigue resistance. A cycle consisted of 1 h at 1100 °C, followed by water cooling to room temperature. The number of thermal cycles in which visible failure of the coatings appeared was measured [5–8].

The residual stresses in the top coat with the variation in the thickness of the bond coat and top coat were calculated using FEM(ANSYS 5.0A). In this study, two-dimensional axi-symmetry was assumed [11, 12]. Fig. 1 shows the model and Table IV shows the bulk value of the material constants of the top coat, bond coat and substrate [13]. The residual stress near the surface of the top coat was measured to confirm the results of FEM by the sine square psi method of XRD [14]. The diffraction of the (4 4 0) plane of stabilized zirconia was used for the measurement.

3. Results and discussion

Fig. 2 shows a cross-sectional scanning electron micrograph of the thermal barrier coating deposited by plasma spraying. The bond coat and top coat were uniformly coated on the substrate. EDS/WDS analysis showed that the compositions of the bond coat and top coat were 72.2Ni–8.8Cr–18.6Al–0.4Y and ZrO_2–8 wt% Y_2O_3, respectively. These compositions were almost the same as those of the powder before spraying. Thermal conductivity of the top coat, measured with the variation of temperature by the laser flash method, was 0.8–1.3 mW K^{-1}, which showed that coatings were properly sprayed.

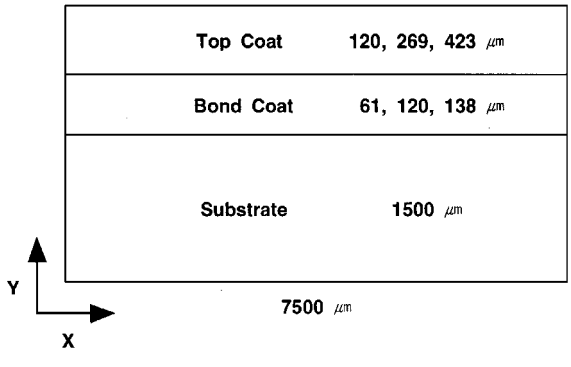

Figure 1 FEM model for thermal barrier coatings.

TABLE IV Material constants of top coat, bond coat, and substrate for FEM analysis

	Top coat	Bond coat	Substrate
Elastic modulus (MPa)	2.412×10^5	1.032×10^4	1.97×10^5
Thermal expansion coefficient ($°C^{-1}$)	7.56×10^{-6}	1.512×10^{-5}	1.51×10^{-5}
Poisson's ratio	0.3	0.3	0.3
Thermal conductivity (W m^{-1} K^{-1})	1.3	91.7	23.7
Specific heat (J kg^{-1} K^{-1})	100	91.7	325

Fig. 3 shows XRD patterns of the top coat powder before plasma spraying (a), the top coat deposited by plasma spraying (b), and the top coat annealed at 1200 °C for 5 h after plasma spraying (c). The top coat powder before plasma spraying was the mixture of monoclinic zirconia and cubic yttria (a). The crystal structure of the deposited top coat was a tetragonal zirconia with a small amount of monoclinic zirconia (b), i.e. the zirconia had reacted with the yttria at high plasma temperature, and stabilized tetragonal zirconia was directly produced by diffusionless shear transformation during cooling to room temperature. This zirconia is quite stable and can be decomposed to the monoclinic phase, but only by heating it to 1400 °C or above for long periods [1]. After annealing for 5 h at 1200 °C, the transformed phase could not be detected (c). Therefore, it could be concluded that the top coat deposited in this study by plasma spraying was stabilized tetragonal zirconia.

Fig. 4 shows the variation of the bond strength as a function of the thickness of the bond coat (a) and top coat (b) of TBCs deposited by plasma spraying. B2T2

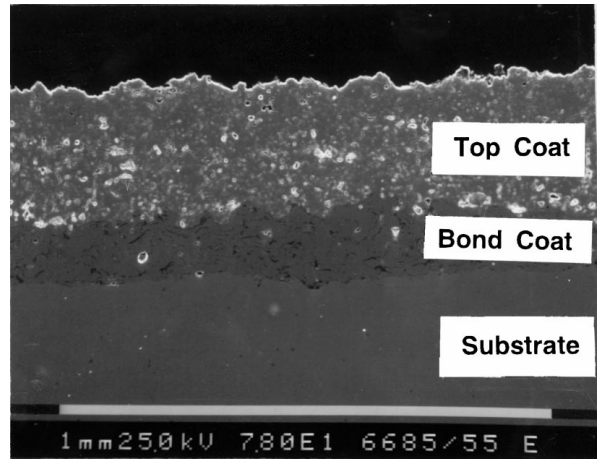

Figure 2 Cross-sectional scanning electron micrograph of thermal barrier coating deposited by plasma spraying.

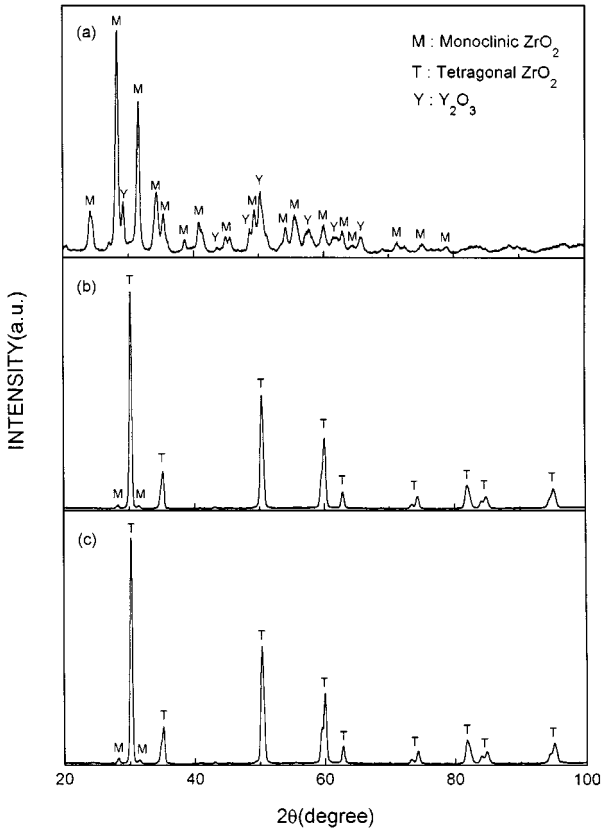

Figure 3 XRD patterns of (a) top coat powder before plasma spraying, (b) top coat deposited by plasma spraying, and (c) top coat annealed at 1200 °C for 5 h after plasma spraying. M, monoclinic ZrO_2; T, tetragonal ZrO_2; Y, Y_2O_3.

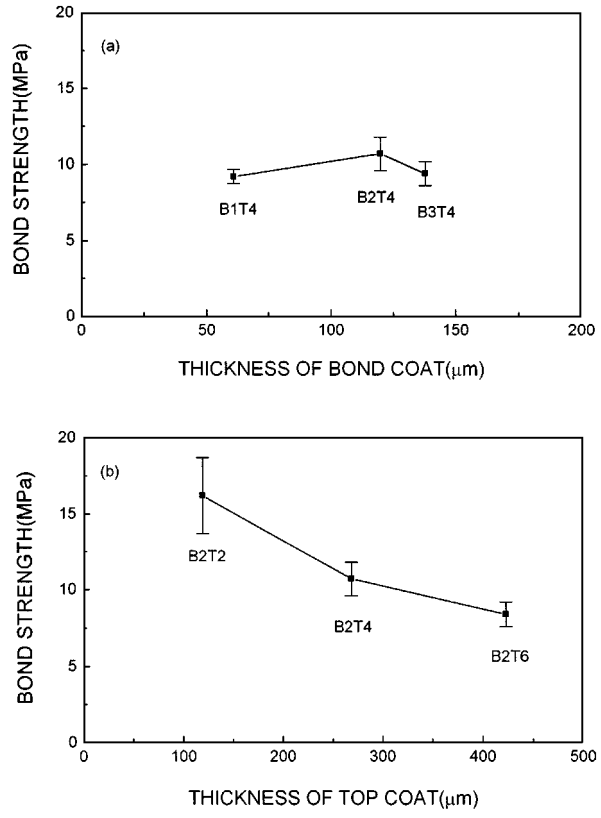

Figure 4 Bond strength as a function of thickness of (a) bond coat and (b) top coat.

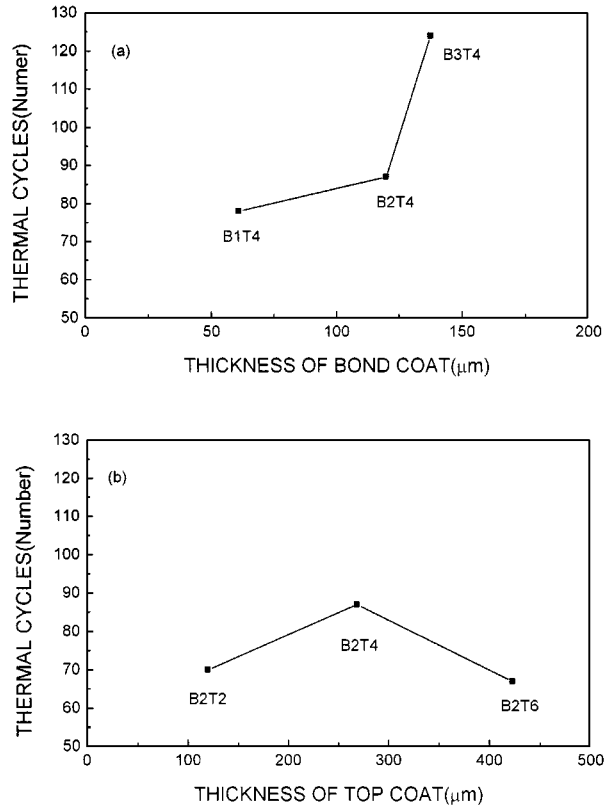

Figure 5 Thermal cycles as a function of thickness of (a) bond coat and (b) top coat.

had a maximum value, and the bond strength decreased with the increase of the thickness of the top coat (b). It was thought that this decrease was due to the increase of residual stress perpendicular to the top coat with the thickness of the top coat.

Fig. 5 shows the variation of the thermal fatigue resistance as a function of thickness of the bond coat (a) and top coat (b) of TBCs deposited by plasma spraying. Thermal cycles in the figure indicate the number of thermal cycles in which visible failure of TBCs was observed. When the thickness of the top coat was constant, the thermal fatigue resistance increased with the increase in the thickness of the bond coat (a). It is well known that the amount of the relaxed thermal stress increases with increasing thickness of the buffer layer. However, TBCs with a constant thickness of bond coat showed a different thermal fatigue characteristic (b). That is, B2T4 had maximum thermal cycles. In the case of the thin top coat, it was thought that bond coat could rapidly react with the oxygen which diffused or penetrated through the porous thin top coat, and TBC with the thick top coat had large thermal stress caused by the difference in temperature between the surface of the top coat and the top coat/bond coat interface.

Residual stress in the top coat was calculated by FEM to explain the above experimental results (Figs 4 and 5). Before the results of FEM calculation were shown, the average stress in the x-direction in the top coat calculated by FEM (Fig. 6) was compared with that measured by XRD (Fig. 7). The average stress in the x-direction was compared because it could only be measured by XRD [14]. X-ray penetration depth, which was calculated using the X-ray absorption coefficient [15] of ZrO_2–8 wt% Y_2O_3, was ~18 μm. Therefore, the

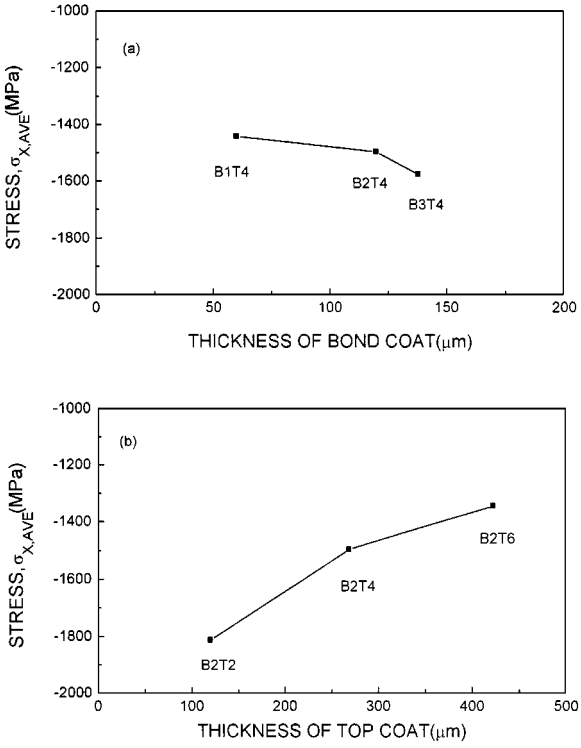

Figure 6 Average stress in the *x*-direction calculated by FEM as a function of thickness of (a) bond coat and (b) top coat.

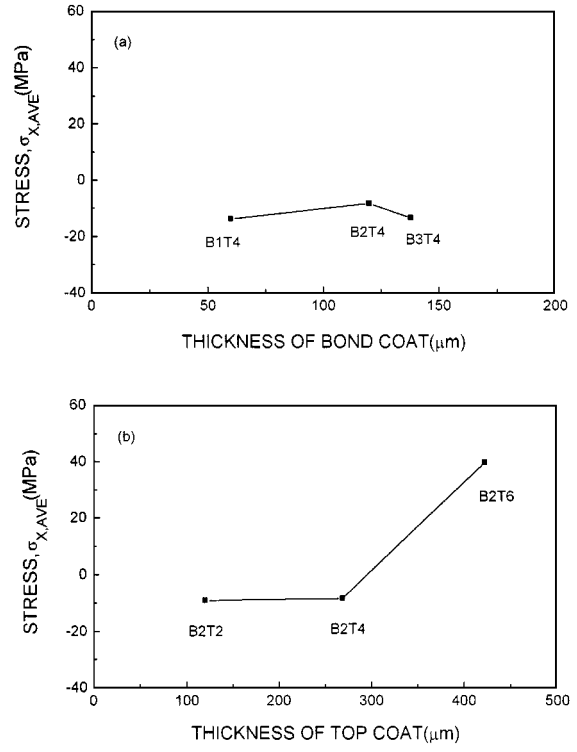

Figure 7 Average stress in the *x*-direction measured by XRD as a function of thickness of (a) bond coat and (b) top coat.

average stress of the *x*-direction in the depth of 18 μm from the surface of the top coat was calculated by FEM. Even though the values of the residual stress in Figs 6 and 7 were different, the tendencies of the variation in the residual stress with the thickness of the bond coat and top coat were similar. Therefore, it could be concluded that FEM analysis was a reasonable method to explain qualitatively the relationship between the thickness of the bond coat and top coat and bond strength (Fig. 4) and thermal fatigue characteristic (Fig. 5).

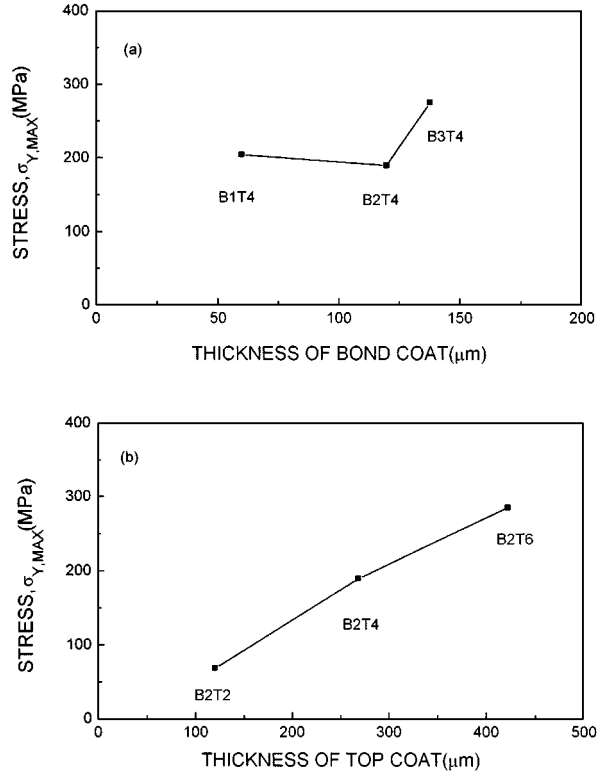

Figure 8 Maximum stress in the *y*-direction calculated by FEM as a function of thickness of (a) bond coat and (b) top coat.

Fig. 8 shows the maximum stress in the *y*-direction which was calculated by FEM to explain the variations in the bond strength with the thickness of the bond coat and top coat. This maximum stress was calculated because the external load was applied to TBC in the *y*-direction when a bond strength was measured. B2T2 had the lowest maximum stress in the *y*-direction (b). Therefore, B2T2 had the highest bond strength (Fig. 4b).

Fig. 9 shows the maximum principal stress which was calculated by FEM to explain the variations in the thermal fatigue resistance with the thickness of the bond coat and top coat. To establish the same condition with that of the experiment, the temperature gradient from the surface of the top coat toward the top coat/bond coat interface was introduced in the calculation. Stress is maximum in the principal direction in which the shear stress component vanishes [16]. Therefore, it was reasonable to calculate the principal stress because no external load was applied when the thermal fatigue was tested. When the thickness of the top coat was constant, the maximum principal stress decreased with the increase of the thickness of the bond coat (a). Consequently, the relationship between the thermal cycles and the thickness of the bond coat shown in Fig. 5a could be explained by the decrease of the maximum principal stress with the thickness of the bond coat. However, in the case of the constant thickness of the bond coat, the maximum principal stress increased with the increase of the thickness of the top coat (b). As mentioned previously, this result showed that the variation of the thermal cycles with the thickness of the top coat shown in Fig. 5b

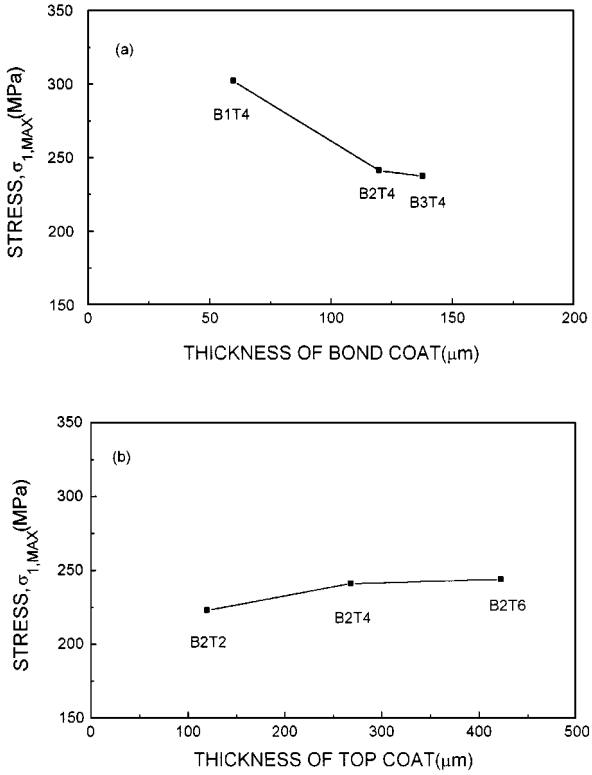

Figure 9 Maximum principal stress calculated by FEM as a function of thickness of (a) bond coat and (b) top coat.

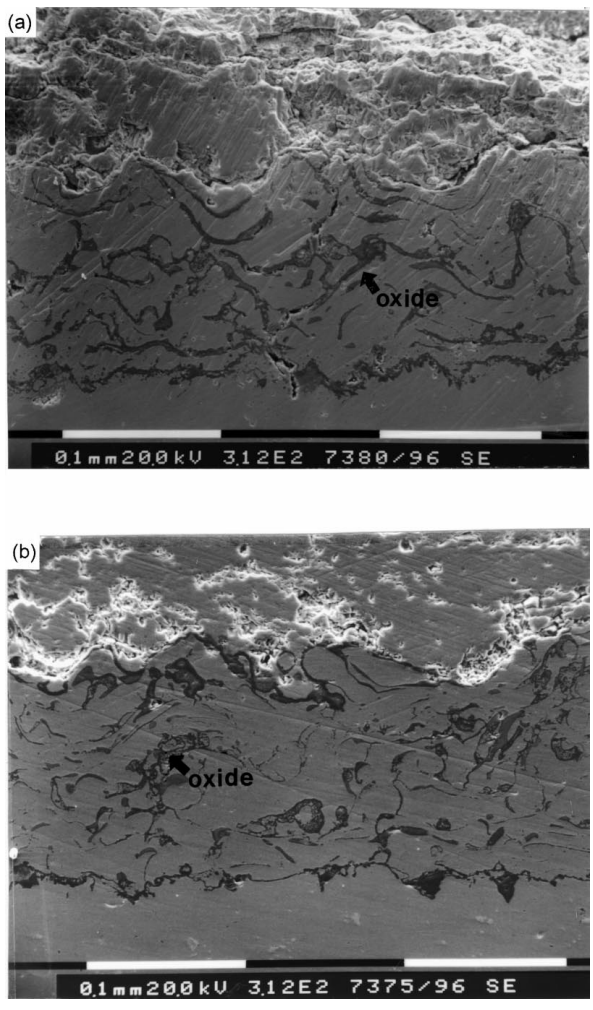

Figure 10 Cross-sectional scanning electron micrographs of the coatings after 50 thermal cycles: (a) B2T2, (b) B2T4.

should be explained by the combination of the oxidation of the bond coat and the residual stress in the top coat. Fig. 10 shows the cross-sectional scanning electron micrographs of the coatings after 50 thermal cycles. As shown in Fig. 10a, B2T2 with the thin top coat revealed that the oxidation of the bond coat occurred rapidly. Consequently, the bond coat could not act as a buffer layer for the relaxation of the thermal stress.

4. Conclusion

NiCrAlY bond coat and ZrO_2–8 wt % Y_2O_3 top coat with various thicknesses were deposited on Hastelloy X by plasma spraying. The compositions of the top coat and bond coat were almost the same as the powder before spraying. The deposited top coat was stabilized tetragonal zirconia and had reasonable thermal conductivity. The bond strength of TBCs increased with a decrease of the maximum residual stress in the *y*-direction in the top coat. The thermal fatigue characteristic increased with decreasing maximum principal residual stress in the top coat and the thickness of oxidation layer of the bond coat.

Acknowledgement

This work was supported by Korea Electric Power Corporation (Grant no. 95-23).

References

1. A. BENETT, *Mater. Sci. Technol.* **2** (1986) 257.
2. P. R. CHALKER, S. J. BULL and D. S. RICHERBY, *Mater. Sci. Eng.* **A140** (1991) 583.
3. Y. MIYAMOTO, T. OKAMOTO, K. YOSHIMOTO and J. HARADA, in "Proceedings of the Satellite Symposium 1 on High Performance Ceramic Films and Coatings of the 7th International Meeting on Modern Ceramics Technologies," edited by P. Vincenzini (Elsevier Science, New York, 1991) p. 57.
4. T. A. TAYLOR, D. L. APPLEBY, A. E. WEATHERILL and J. GRIFFITHS, *Surf. Coat. Technol.* **43/44** (1990) 470.
5. B. C. WU, E. CHANG, S. F. CHANG and C. H. CHAO, *Thin Solid Films* **172** (1989) 185.
6. R. D. MAIER, C. M. SHEUERMANN and C. W. ANDREWS, *Am. Ceram. Soc. Bull.* **60** (1981) 555.
7. S. F. CHANG, C. H. CHAO, B. C. WU, R. Q. LEU and E. CHANG, *J. Vac. Sci. Technol.* **A9** (1991) 2099.
8. Y. K. PARK, MS thesis, Department of Metallurgical Engineering, Yon Sei University, Seoul, Korea (1991).
9. R. MCPHERSON, *Thin Solid Films* **112** (1984) 89.
10. M. C. RADHAKRISHNA, H. J. DOERR, C. V. DESHDANDEY and R. F. BUNSHAH, *Surf. Coat. Technol.* **36** (1988) 143.
11. S. Y. KWEON and S. K. CHOI, *Scripta Metall. Mater.* **32** (1995) 359.
12. M. NISHIDA and T. HANABUSA, in "Proceedings of the 14th International Thermal Spray Conference," edited by A. Ohmori (High Temperature Society of Japan, Osaka, Japan, 1995) p. 915.
13. A. J. MOSES, in "The practicing scientist's handbook" (Van Nostrand Reinhold, New York, 1978).
14. I. C. NOYAN and J. B. COHEN, in "Residual stress" (Springer, New York, 1987).
15. CULITY, in "Elements of X-ray diffraction" (Addison-Wesley, Reading, MA, 1978).
16. J. F. NYE, in "Physical properties of crystals" (Oxford University Press, London, 1967).

Received 17 December 1996
and accepted 23 July 1998